Vol 12 No 2, February 2003
1009-1963/2003/12(02)/0189-09

Chinese Physics

© 2003 Chin. Phys. Soc.
and IOP Publishing Ltd

Bursty events and incremental diffusion in a local diffusion and multi-scale convection system*

Xu Guo-Sheng(徐国盛), Wan Bao-Nian(万宝年), and Song Mei(宋 梅)

Institute of Plasma Physics, Chinese Academy of Sciences, Hefei 230031, *China*

(Received 17 July 2002; revised manuscript received 14 October 2002)

A one-dimensional cellular automaton is defined without the critical gradient rule ($\Delta h > \Delta h_c$) which is essential to the existence of avalanches in self-organized criticality (SOC) models. Instead, only the local diffusion rule is used, however, the characteristics of SOC, such as the bursty behaviour, power-law decay in fluctuation spectra, self-similarity over a broad range of scales and long-time correlations, are still observed in these numerical experiments. This numerical model is established to suggest that the bursty events and the incremental diffusion observed universally in fusion experiments do not necessarily imply the submarginal dynamics.

Keywords: bursty events, incremental diffusion, self-organized criticality, cellular automata
PACC: 5225, 5255

1. Introduction

Anomalous transport in fusion plasmas is generally believed to be driven by plasma turbulence.[1] Most turbulent transport models are based on random diffusion due to fluctuations on a microscopic scale, leading to the gyro-Bohm scaling.[2−4] However, detailed experimental studies revealed that the dominant transport scalings are between Bohm and gyro-Bohm,[5] which implies the existence of large-scale transport mechanisms. It is commonly observed that the plasma parameters, such as density and temperature, exhibit large fluctuations with 'bursts'.[6] These turbulent phenomena characterized by radial fast propagation cannot be easily understood in a diffusive framework. To shed some light on these apparent discrepancies between theory and experiment, the models based on self-organized criticality (SOC) were proposed, suggesting the presence of avalanches that occur on all spatial and temporal scales, including radial scales up to the system size.[7−9] Consequently, the associated loss of confinement is caused by non-local convection in addition to diffusion. Bursty behaviour, power-law decay in fluctuation spectra, self-similarity over a broad range of scales, long-time correlations and plasma-profile resilience observed in many experiments[10−17] have been found consistent with some SOC predictions, although some authors[18,19] reported long-range correlations also for non-SOC systems.

Using SOC concept to explain bursty events and incremental diffusion implies the submarginal dynamics,[20−23] thereby in SOC models, that the critical gradient rule ($\Delta h > \Delta h_c$) is essential to the existence of avalanches.[24,25] It suggests that SOC can only account for the bursty behaviour near the marginal stable state of the candidate instabilities. However, unfortunately, all of the instability mechanisms suffer from the drawback that, experimentally, the Bohm scaling and bursty events can be observed with the profiles seemingly to be stable to the candidate mode over much, if not all, of the radius.[24,25] How to explain the bursty phenomena in the state far below the stability threshold? And whether the presence of bursts necessarily implies the submarginal dynamics? This paper will give a one-dimensional cellular automaton without the critical gradient rule, instead, only the local diffusion rule is used. However, the characteristics of SOC, such as the bursty behaviour, power-law decay in fluctuation spectra, self-similarity over a broad range of scales and long-time correlation, are still observed in these numerical experiments. In a steady state, this simple model can give the multi-scale fluctuations sharing the radial dispersion relation similar to that observed in fusion plas-

*Project supported by the National Natural Science Foundation of China (Grant No 10175069) and by the Chinese Academy of Sciences (Grant No 01062025).

mas. Perturbative transport analysis indicates that there is a transient enhancement of diffusivity during the burst propagating radially, which results in a greater incremental diffusivity than the power-balance diffusivity ($D^{\rm hp} > D^{\rm pb}$), especially in the edge region. This numerical model is established to give a new transport understanding, i.e. the local diffusion and multi-scale convection. In this model the diffusion is manifested as the local diffusion and the down hill unilateral iteration process. This suggests that the bursty events and the incremental diffusion universally observed in fusion experiments do not necessarily imply the submarginal dynamics.

2.Description of the cellular automaton

The cellular automaton algorithm is defined as follows. Similar to the running sand pile model,[7−9] the domain is divided into cells $R = \{r|0, 1, 2, \cdots, a\}$ which are evolved in steps. The symbol $h_{r,t}$ is the height of cell r in step t. Because the cellular automaton model presented here is purely a numerical model, all quantities in this model are dimensionless quantities. The system starts with the initial state $h_{r,0}$=0 ($r \in R$). Firstly, two kinds of sources are added to the cells. One is the average source with a profile A_r ($r \in R$) and the other is the noise source with a profile N_r ($r \in R$). A random number generator generates a cluster of normal distribution random numbers $n_{r,t}$ ($r \in R$) (white noise signal) with a mathematical expectation =0 and variance =1 in step t (the reliability of the random number generator will be proved in section 3). The total source $s_{r,t} = A_r + N_r n_{r,t}$ ($r \in R$) is deposited to the cells according to $h_{r,t} = h_{r,t-1} + s_{r,t}$ ($r \in R$). Next, the transport following the local diffusion rule takes place from r=1 to a, or reverse. The algorithm is

$$\Gamma_{r,t} = D_r(h_{r-1,t} - h_{r,t}),$$

$$h_{r-1,t} = h_{r-1,t} - \Gamma_{r,t},$$

$$h_{r,t} = h_{r,t} + \Gamma_{r,t}.$$

Here, $\Gamma_{r,t}$ is the flux at cell r in step t, and D_r is the local diffusivity at cell r. Finally, the boundary conditions ($h_{0,t} = h_{-1,t}$ and $h_{a,t}$=0) are applied, i.e. the mass can only flow out of the system from the $r = a$ side. Then step t is completed and step $t + 1$ begins. In terms of corresponding physical quantities which we relate with turbulent systems, each cell can be thought of as the location of a local turbulent eddy. The average profile h_r is equivalent to the mean density or temperature profile, while the total mass $\sum_r h_r$ is the total particle or energy content of the system. The flux Γ_r is clearly the particle or heat flux. The average source corresponds to the gas puffing or heating, and the noise source acts as the background fluctuations. With these assumptions, the system evolves of itself and after a transient state it reaches a steady state in which the input is on average balanced by the drainage at the open boundary. The transport in this model contains two kinds of processes, which combine to make a complex transport system. For a local scale, the transport between two neighbouring cells is a linear diffusion process $\Gamma_r = D_r \Delta h_r$ with an in–out symmetry. This means that mass can diffuse inward or outward, depending on the local gradient Δh_r. The local diffusion can be understood as the result of local random walks driven by turbulence on a microscopic scale. Obviously, the transport dynamics described here is independent of the underlying specific local instability. For scales larger than two neighbouring cells, the group effect of the local diffusion produces a new transport behaviour, the "multi-scale convection". In this model it is manifested as a downhill unilateral iteration process. Although it is very similar to diffusion, it is not an ordinary diffusion process. Because diffusion is a process in which transport takes place at every radial location simultaneously, however, in this model the large-scale transport proceeds cell-by-cell and step-by-step. One can compare it with a discrete diffusion system to find the subtle difference. Thus, it is a transport system in which the linear diffusion process takes place only in local scale, and for large scales the multi-scale convection works. Comparing it with a SOC sand pile, we can find the only essential replacement is the local transport rule. The multi-scale convection and the SOC sand pile have the same downhill unilateral iteration process and the similar source loading process. We will demonstrate that the unilateral iteration process rather than the critical gradient rule is responsible for the avalanches in SOC models.

Numerical experiments are carried out with the simplest parameters: a=50, A_r=0.1, N_r=1 and D_r=0.5 ($r \in R$), which denotes that the effect of local diffusion is to flatten the local profile. This is consistent with the idea contained in the simple mixing length estimate.

3. Steady-state transport analysis

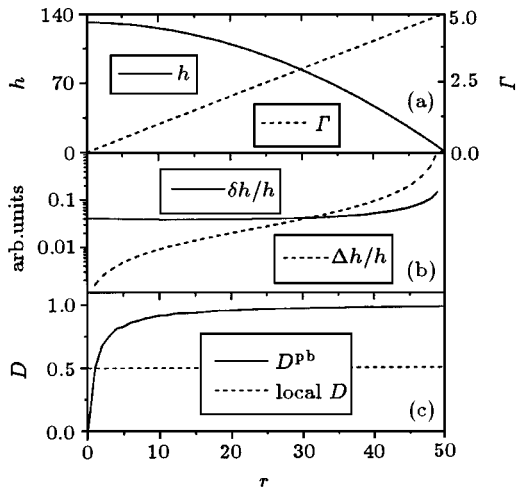


Fig.1. The time-averaged profiles in steady state, (a) the height h_r and the flux Γ_r, (b) the relative fluctuation level $\delta h/h$ and the inverse gradient length $\Delta h/h$, (c) the local diffusivity D_r and the power-balance diffusivity which is defined as $D^{\rm pb}_{r,t} = \Gamma_{r,t}/(h_{r-1,t} - h_{r,t})$, where $h_{r-1,t}$ and $h_{r,t}$ use the final value after step t has been finished.

Figure 1 shows the time-averaged profiles in a steady state, all these profiles being averaged over 10^4 time steps after saturation is reached. In Fig.1(a), the height h_r exhibits a parabola profile, which is the result of spontaneous evolution. The flux Γ_r increases linearly outward. Figure 1 (b) shows the relative fluctuation level $\delta h/h$ and the inverse gradient length $\Delta h/h$, where δh is the fluctuation level and Δh is the difference between two neighbours h_{r-1} and h_r. The outward increase of the relative fluctuation level in the edge region is dominated by the decrease of the height, which is similar to the case in experimental edge plasmas. The gradient of the height h_r supplies the free energy consumed by local diffusion, and the fluctuations are not only driven by the background noise but also influenced by the transport process. So the fluctuation level is much larger than the random variations (N_r=1) applied to this model. The profile of inverse gradient length is determined only by the profile of local diffusivity. Although in this system the transport process is composed of local diffusion and multi-scale convection, we still can calculate the power-balance diffusivity or effective diffusivity. We can treat it as a pure diffusion system to calculate the diffusivity, just as we can calculate the transport coefficient of turbulent plasma while we do not consider the underlying mechanism. Figure 1 (c) shows the local diffusivity D_r=0.5 and the power-balance diffusivity or effective diffusivity which is defined as $D^{\rm pb}_{r,t} = \Gamma_{r,t}/(h_{r-1,t} - h_{r,t})$, where for $h_{r-1,t}$ and $h_{r,t}$ we use the final values after step t has been finished. The power-balance diffusivity is larger than the local one, and it increases outward. The distinction between the two kinds of diffusivity gives the picture that the interaction between the local diffusions from different radial locations can generate an additional macroscopic transport. The cell size is of a local transport scale or local fluctuation scale. The existence of an additional global transport signifies that there exists a much longer transport scale than the cell size. This long-scale transport is the group effect of the local diffusion which results from the unilateral iteration process. The mass and information can be convected to various radial locations in a single time step. This multi-scale convection mechanism cannot be found in an ordinary diffusion system; however, it brings us an alternative explanation to the bursty events and the incremental diffusion observed in turbulent plasma experiments. The profiles of power-balance diffusivity and average source can explain the profiles of height and flux shown in Fig.1(a).

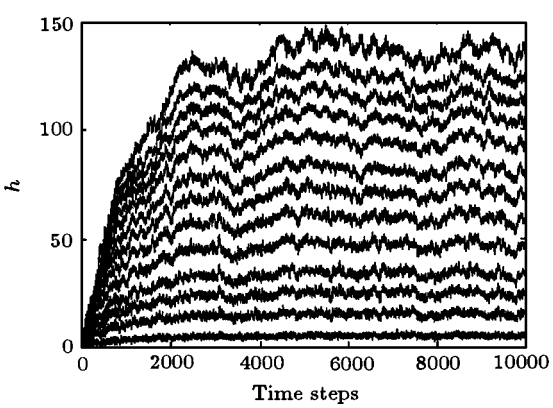


Fig.2. The history of height $h_{r,t}$ for 10^4 time steps at several radial locations: the curves from top to bottom of the figure correspond to r=0, 14, 19, 23, 27, 31, 34, 37, 40, 43, 45, 47, 49.

In Fig.2, the history of height $h_{r,t}$ for 10^4 time steps at several radial locations is presented. The relaxation from the initial profile to the steady profile can be seen in time evolution. The steady state will not be reached until the height saturates at approximately 5000 time steps. It shows fluctuations on all spatial and temporal scales, including large scales up to the system size. It is not difficult to find some large-scale bursty events propagating radially with a

very long correlation length. These coherent events can be seen to grow and shrink, displaying various radial sizes and lasting various lengths of time. Some are seen to propagate up hill, while others propagate down hill or in both directions. It should be kept in mind that the average flux always moves down hill. The upward propagation includes a void moving up by symmetry, which is the same as a bump moving down. This dual-propagation is a signature shared with SOC systems.

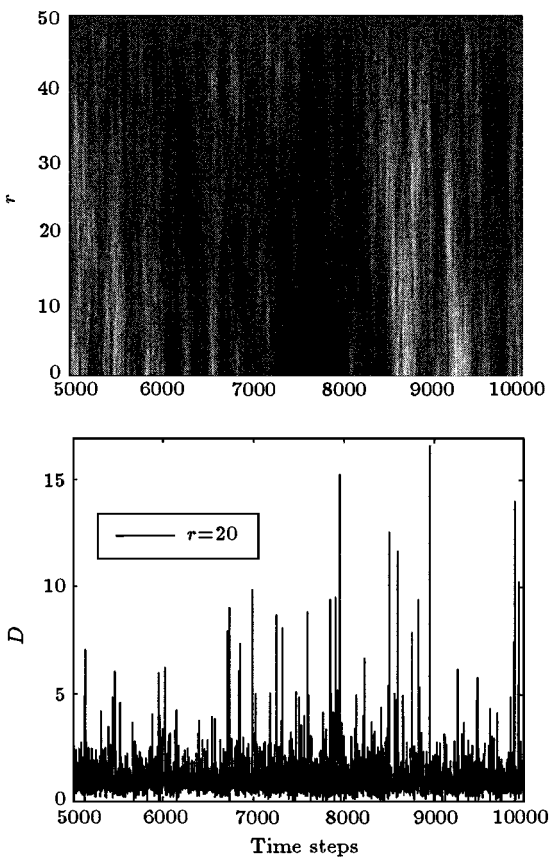


Fig.3. The pseudo colour image of mean removed height fluctuations $\delta h_{r,t}$ and the power-balance diffusivity at r=20 with the same data plotted in Fig.2.

Fig. 3 presents the pseudo-colour image of mean removed fluctuations $\delta h_{r,t}$ and the power-balance diffusivity at r=20 with the same data plotted in Fig.2. We can find the bursts on various scales ballistically propagating in radial directions. The clear coherent structures form under the macroscopic effect of interaction between local diffusion cells. Both positive and negative disturbances can be seen to move radially with various scales. The local diffusion between two neighbouring cells determines the smallest transport scale, and these local transport cells structure the global events with group effects. The power-balance diffusivity brings about the bursty behaviour, demonstrating that the bursty events can intermittently enhance the transport ability of a turbulent system. The enhancement of diffusivity is the result of multi-scale convection.

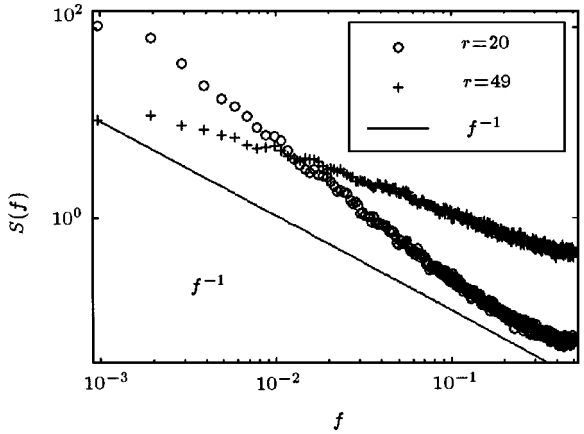


Fig.4. The fluctuation spectra of $\delta h_{r,t}$ at r=20 and 49 respectively. The solid line denotes f^{-1} decay, with the sampling frequency =1.

Figure 4 displays the power-law decay in the fluctuation spectra. The fluctuations are $\delta h_{r,t}$ at r=20 and 49. The solid line denotes f^{-1} decay. The power-law decay in the auto-power frequency spectrum implies that the saturated fluctuations have broad time scales and the fluctuation energy dissipates in the high-frequency region. The spectral falloff is approximately f^{-1}, which is analogous to the situation in the overlapping avalanche region of SOC models. The transport events with different scales interact with each other to give multi-layer coherent structures. In the lowest frequency region the spectral power is relatively flat. This region is identified with global discharge events that have extremely long correlation time. It is easiest to see these discharge events by looking at the time history of mean removed height fluctuations in Fig.3.

Figure 5 is plotted to support the existence of self-similarity and long-time correlation. To carry out the analysis of the probability density function (PDF) of $\delta h_{r,t}$ on different time scales, the wavelet decomposition is used.[26,27] We choose N=44 wavelets as in Ref.[28]. To accumulate sufficient statistics, the system is iterated for 6×10^5 time steps after saturation is reached. To compare the shape of the PDF on different scales, for each time scale the coefficients $\delta h_{r,t}(\tau)$ have been normalized by the standard deviation $\delta h_{r,t}(\tau)/\sigma(\tau)$. In the calculation of PDFs, we change the time resolution by a factor of 2. In this way, the largest scale that we can investigate is up to

τ=4096 time steps. We cannot make a time resolution above this value, because there are not enough points left to calculate a PDF. So we can have 12 time scales ($1 \leq \tau \leq 2^{12}$). The left-hand side two plots of Fig.5 show PDFs at r=20 and 49. The PDFs from the 12 time scales are plotted together and fall on top of each other, which indicates the presence of self-similarity. The middle two plots display the relative standard deviation $\sigma(\tau)/\sigma(1)$ as a function of time scales at r=20 and 49. The self-similarity range is about $1 \leq \tau \leq 2^8$. The right-hand side two plots present the Hurst exponent $H(\tau)$ as a function of time scales. $H(\tau)$ is defined as $\sigma(\tau)/\sigma(1) = \tau^{H(\tau)-1}$.[29,30] We can see that $H(\tau)$ is close to 1 at r=20 and close to 0.8 at r=49, which are meaningfully greater than the trivial value H=0.5. This result gives the evidence of long-time correlations.

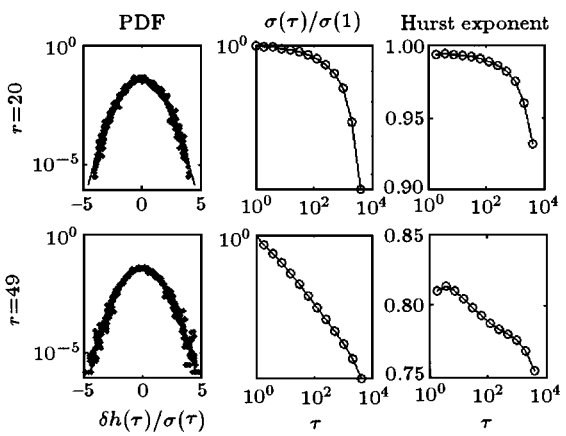


Fig.5. The left-hand side two plots show PDFs of height fluctuations $\delta h_{r,t}$ on 12 different time scales at r=20 and 49; the middle two plots display the relative standard deviation $\sigma(\tau)/\sigma(1)$ as a function of time scales at r=20 and 49; the right-hand side two plots give the Hurst exponent $H(\tau)$ as a function of time scales at r=20 and 49. $H(\tau)$ is defined as $\sigma(\tau)/\sigma(1) = \tau^{H(\tau)-1}$.

In a one-dimensional turbulent system, a transport process usually accompanies fluctuations which propagate radially. The radial correlativity and propagating capability of fluctuations are associated with time and space scales. In Fig.6, the typical radial normalized dispersion relation of fluctuations is provided as a pseudo colour image. The standard two-point statistic correlation-analysis technique[31] is used. The two signals are probed at two nearest radial locations (r=49 and 48). To accumulate sufficient statistics, the system is iterated for 1×10^5 time steps after saturation is reached. This dispersion relation is quite similar to the experimental results measured in the edge plasma with radial-separated or poloidal-separated Langmuir probes.[32] For example, there is a strong coherence in the low-frequency and small wavenumber region, and the coherence decays toward the high-frequency and large wavenumber region, where an obvious propagation feature can be found. These denote that the fluctuations with a longer time scale and a broader space scale have stronger coherence. The existence of much more comparability implies that the fluctuation phenomena described by so simple a numerical model may share the same structure of plasma turbulence.

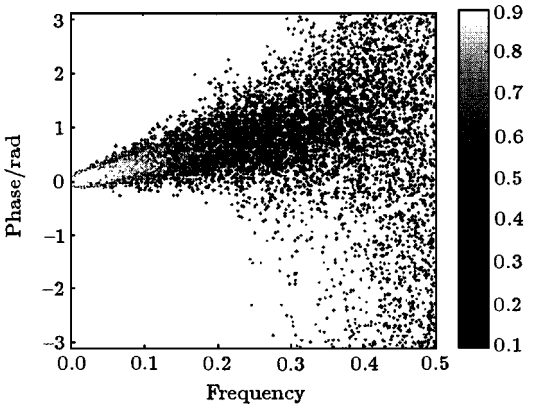


Fig.6. The pseudo colour image of typical radial normalized dispersion relation of fluctuations. The two signals are probed at two nearest radial locations (r=49 and 48).

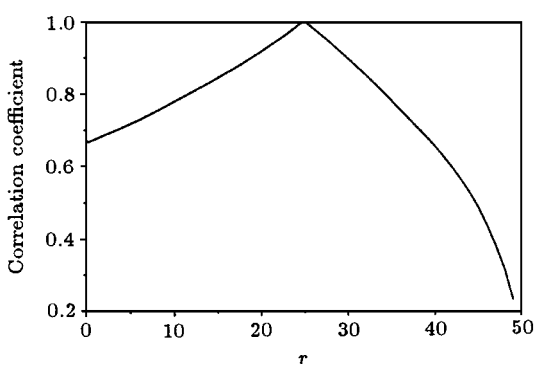


Fig.7. The profile of correlation coefficients between height $h_{25,t}$ and $h_{r,t}$ ($r \in R$) with the same data as in Fig.6.

Figure 7 shows the profile of correlation coefficients between height $h_{25,t}$ and $h_{r,t}$ ($r \in R$) with the same data as in Fig.6. The correlation decreases with the radial distance between two radial locations, and there is an asymmetry between the in side and outside of the r=25 location. A stronger correlation appears in the centre than at the edge. These suggest that, when we increase the radial distance between the two

locations, small-scale fluctuations will lose their correlation quickly, and only the large-scale fluctuations keep the memory of perturbation information during their propagating radially.

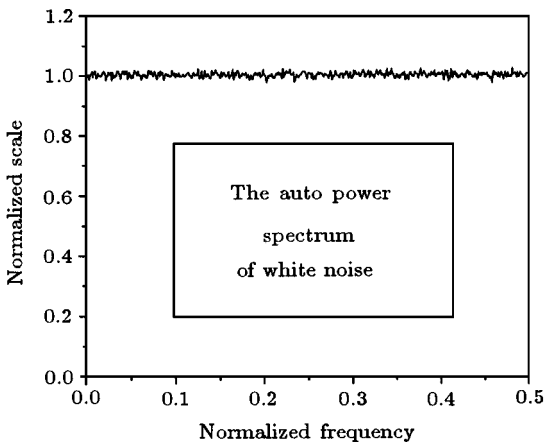


Fig.8. The normalized auto-power spectrum of the white noise (10^7 points) generated by the random number generator.

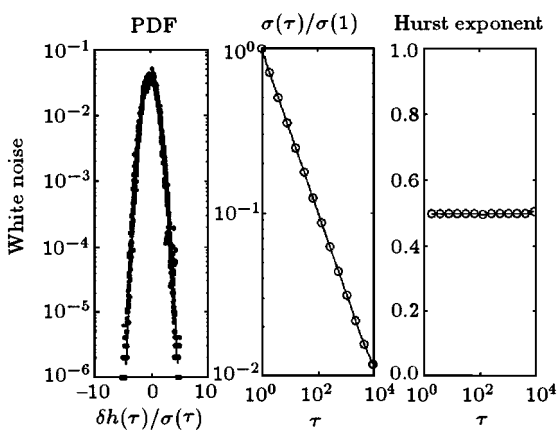


Fig.9. The PDF and Hurst exponents of the white noise (10^6 points) generated by the random number generator using the same wavelet decomposition method described above. The left-hand side plot shows PDF on 12 different time scales. The middle plot displays the relative standard deviation $\sigma(\tau)/\sigma(1)$ as a function of time scales. The right-hand side plot gives the Hurst exponent $H(\tau)$ as a function of time scales.

Since we are using a huge number of random numbers, the reliability of the random number generator is necessary. Figure 8 shows the normalized auto-power spectrum of the white noise (10^7 points) generated by the random number generator. It is equal to unity in the entire frequency domain. Figure 9 plots the PDF and Hurst exponents of the white noise (10^6 points) using the same wavelet decomposition method described above. The PDF fits the Gaussian distribution quite well and the Hurst exponents are approximately equal to 0.5 in all scales, indicating that it is almost a perfect random number generator.

4. Perturbative transport analysis

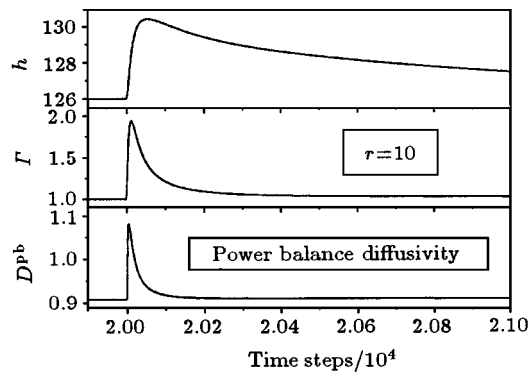


Fig.10. The waveforms of height $h_{10,t}$, flux $\Gamma_{10,t}$ and power-balance diffusivity $D^{\rm pb}_{10,t}$ versus time steps at location r=10.

The time-to-peak analysis technique[33] is used to investigate the transitional response of the one-dimensional cellular automaton to a pulse perturbation. The time-to-peak method devised by Soler and Callen (1979)[34] is the simplest for the analysis of the sawtooth heat-pulse propagation; however, it assumes a cylindrical geometry. For a one-dimensional system, the problem becomes simpler. In order to give prominence to the influence of perturbation, the noise source has been removed, i.e. N_r=0 ($r \in R$). The system starts with the initial state $h_{r,0}$=0 ($r \in R$) and after 10000 time steps a steady state is reached. At the moment of the $20000^{\rm th}$ time step, an instant pulse is added to the system at the centre location of r=0 ($h_{0,20000} = h_{0,19999}$+100). This pulse quickly propagates outward. Since a pulse function contains plenty of fluctuation information, the response of the system to the pulse function reflect actually the radial propagation of fluctuations with various frequencies. Figure 10 shows the waveforms versus time steps at the location r=10. The height $h_{10,t}$ comes to its peak after 55 time steps, and then decays. The flux $\Gamma_{10,t}$ reaches its peak after 12 time steps, it seems to response more rapidly. $D^{\rm pb}_{10,t}$ is the power-balance diffusivity or effective diffusivity, which has been defined in section 3. It comes to its maximum only after six time steps. The transient enhancement of diffusivity during the burst propagating radially is due to the multi-scale convection mechanism, which combines a rapid (one time step) response with more diffusive behaviours.

We should emphasize that it is not a diffusion system, and it contains convection; however, we still can calculate the diffusivity, just as we can calculate the transport coefficient of a turbulent plasma when we do not know the underlying mechanism.

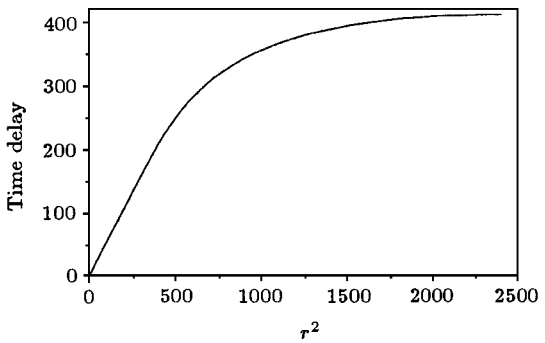


Fig.11. The decay time $t_{\rm p}$ at which the height $h_{r,t}$ perturbation reaches its peak, plotted as a function of the square of minor radius r^2.

In Fig.11, the decay time $t_{\rm p}$ at which the perturbation with height $h_{r,t}$ reaches its peak is plotted as a function of the square of minor radius r^2. Apparently, diffusion characterizes the process of burst propagation. Approximate linear variation can only be found in the range $10 < r < 20$.

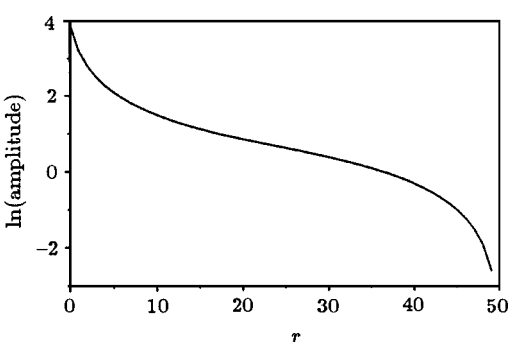


Fig.12. The natural logarithms of the amplitude of perturbation peak $\ln h_{\rm p}$ versus minor radius r.

Fig. 12 illustrates the natural logarithms of the amplitude of the perturbation peak $\ln h_{\rm p}$ versus the minor radius r. Exponential decay can be satisfied only in the middle range of $15 < r < 30$. Since the time-to-peak method assumes that the diffusivity is constant in the range from the mixing radius to the measured location r, we can obtain an averaged diffusivity over that region. A more precise extension of the time-to-peak model given by Lopes Cardozo *et al*[33] gives a more localized evaluation of diffusivity. The following approximate formula is used[33]

$$D_r^{\rm TTP} = v_{\rm p} \times \lambda, \quad v_{\rm p} = \left(\frac{\partial t_{\rm p}}{\partial r}\right)^{-1}, \quad \lambda = \left(\frac{\partial \ln h_{\rm p}}{\partial r}\right)^{-1},$$

where $v_{\rm p}$ is the propagation velocity and λ is the decay length of the perturbation peak.

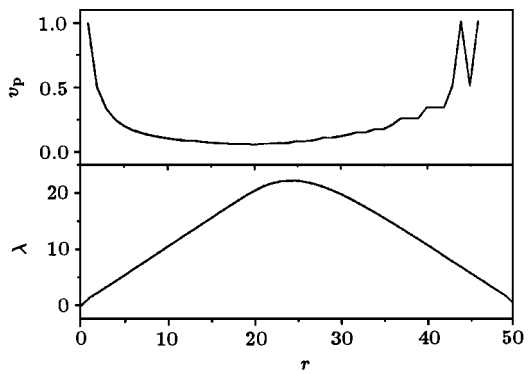


Fig.13. The propagation velocity of peak $v_{\rm p}$ and the decay length of peak λ versus minor radius r.

Figure 13 shows the propagation velocity $v_{\rm p}$ and the decay length of the perturbation peak λ versus the minor radius r. The relation is nonlinear and the burst propagates faster in the centre and in the edge regions, where the decay length is shorter. This indicates that there is a nonlinear process during the burst propagation. Firstly, the burst decelerates and then accelerates. Figure 14 shows that the profile of diffusion coefficient $D_r^{\rm pb}$ is the power-balance diffusivity or effective diffusivity, which has been defined in section 3. $D_r^{\rm hp}$ is the time-to-peak analysis diffusivity defined as $D_r^{\rm hp}=r^2/t_p$ (only for a one-dimensional system). In the interior region we have $D_r^{\rm hp} \approx 2D_r^{\rm pb}$, while in the exterior region $D_r^{\rm hp} \gg D_r^{\rm pb}$ and they all increase outward. Recalling that in Fig.1 (a) the exterior region is steeper, similar to the situation in the plasma edge where turbulence simulations and fluctuation measurements indicate that there exist large-scale transport events. $D_r^{\rm TTP}$ is the diffusivity from the extension of the time-to-peak method. In the interior region, $D_r^{\rm TTP}$ is close to $D_r^{\rm pb}$; however, in the exterior region, $D_r^{\rm TTP}$ is close to $D_r^{\rm hp}$ with $D_r^{\rm TTP} > D_r^{\rm pb}$. The reason for the unsmooth of the $D_r^{\rm TTP}$ curve is due to the radial discretization in a numerical model. If the radial resolution increases, the $D_r^{\rm TTP}$ curve will be smoother, but this does not affect our conclusion. The incremental diffusion is the natural result of the transport dynamics described in this model.

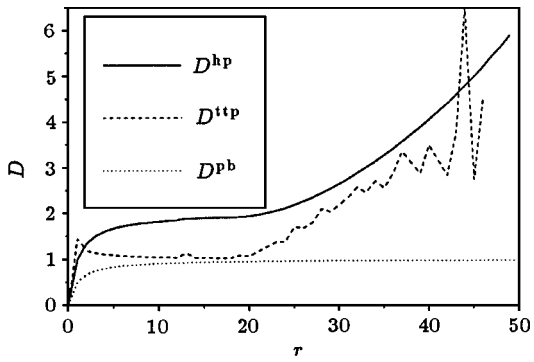


Fig.14. The profiles of diffusion coefficient. $D_r^{\rm pb}$ is the power-balance diffusivity. $D_r^{\rm hp}$ is the time-to-peak analysis diffusivity. $D_r^{\rm TTP}$ is the diffusivity from the extended time-to-peak method.

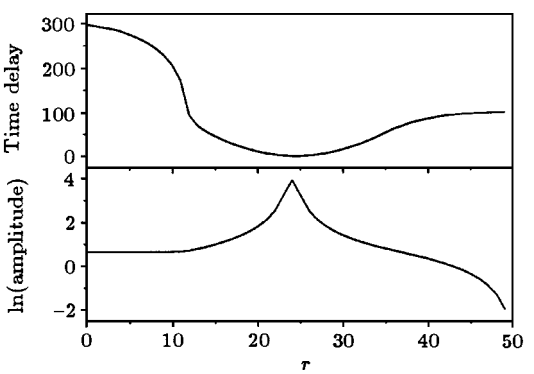


Fig.15. The decay time $t_{\rm p}$ at which the height $h_{r,t}$ perturbation reaches its peak and the natural logarithms of the amplitude of perturbation peak ($\ln h_{\rm p}$) versus the minor radius r.

From the foregoing analysis, we can find many nonlinear features of this system. Here, we point out another characteristic, e.g. in–out asymmetry. The model we proposed has an intrinsic in–out asymmetry caused by the ordering of the iterations. Mass and in formation can propagate out to the edge on a single time step, whereas they can move inwards only one spatial cell per time step (when the ordering of the iteration is outward). Along the direction of iteration (for example outward) the transport is enhanced, and this produces an incremental diffusion. The unilateral enhancement of the transport is the result of unilateral iteration process. In order to demonstrate the in–out asymmetry, what we should do is to compare between pulses propagating inward and outward. We replace the pulse at centre location r=0 with a pulse at the location of r=25 at the $20000^{\rm th}$ time step in the numerical experiment described above ($h_{25,20000} = h_{25,19999}$+100). This pulse quickly propagates. The results from the time-to-peak analysis are plotted in Fig.15. Both the time and amplitude decays show an in–out asymmetry with respect to burst propagation, which indicates a high transport for an outward propagating pulse and a low transport for an inward propagating pulse. These phenomena have really been observed in recent fusion experiment.[35]

5. Discussions and conclusions

For two decades, the propagation of pulse in fusion plasma have been observed to be diffusive in all kinds of perturbative transport experiments, but apparently governed by a transport coefficient about two times larger than that governing the background plasma. Whether there exists a critical gradient (or gradient length) independent of diffusion, which governs transport, is a fundamental transport problem. It has recently become the subject of intense interest and investigation in magnetic confinement physics.[36,37] While many anomalous transport theories and experiments try to support the existence of critical threshold, there are good reasons to believe it is too early to pass the opinion. For example, we all know that convection exists in a turbulent plasma, however, we are not clear how it works. The influences of convection on the diffusion process and the interaction between local scale and global scale are still not clear at all. We believe that these questions are closely related to the mechanism underlying the bursty events and the incremental diffusion.

The universality of the large-scale cross-field $\boldsymbol{E} \times \boldsymbol{B}$ convective transport has been established for a long time.[38–41] And there is an extensive body of work imaging the edge of various devices with fast cameras,[42,43] which show that moving plasma filaments exist in the edge region. Thus, the work over the years has accumulated overwhelming evidence that moving coherent structures are convected in the edge region of the magnetically confined plasmas carrying a large amount of the total transport. But what are the underlying sources for this fast convective transport is still not clear. Because bursts are often reported in SOC far from the last closed flux surface where the density and temperature profiles are rather flat,[39] indicating that the underlying mechanism may not be SOC, since avalanches are expected to propagate radially in regions where gradients are close to marginal. A different explanation is needed. The turbulence spectra measured in a fusion plasma always present stronger coherence for longer time scale and broader space scale, so we have to

think that large-scale coherent structures may be an intrinsic characteristic of this kind of system. Hence in this work, a simplest numerical diffusion model is used to give prominence to the elementary features of plasma cross-field transport, such as the local diffusion and the multi-scale convection. And we give the evidence that this transport mechanism can generate incremental diffusion during the burst propagating radially, which results in the formation of large-scale radial structures and additional convective transport. This is presented as an alternative explanation for the existence of the large-scale cross-field convective transport in fusion plasmas.

In conclusion, a one-dimensional cellular automaton is defined without the critical gradient rule ($\Delta h > \Delta h_c$) which is essential to the existence of avalanches in the SOC models. Instead, only the local diffusion rule is used, however, the characteristics of SOC, such as the bursty behaviour, power-law decay in fluctuation spectra, self-similarity over a broad range of scales and long-time correlations, are still observed in these numerical experiments. In a steady state, this simple model can give the multi-scale fluctuations sharing the radial dispersion relation similar to that observed in a fusion plasma. Perturbative transport analysis indicates that there is a transient enhancement of diffusivity during the burst propagating radially, which results in a greater incremental diffusivity than the power-balance diffusivity ($D^{\rm hp} > D^{\rm pb}$), especially in the edge region. This numerical model is established to give a new transport understanding, i.e. the local diffusion and multi-scale convection. In this model the diffusion is manifested as the local diffusion and the down hill unilateral iteration process. This suggests that the bursty events and the incremental diffusion observed universally in fusion experiments do not necessarily imply the submarginal dynamics.

References

[1] Carreras B A 1997 *IEEE Trans. Plasma Sci.* **25** 1281
[2] Kadomtsev B B 1965 *Plasma Turbulence* (London: Academic)
[3] Connor J W and Wilson H R 1994 *Plasma Phys. Controlled Fusion* **36** 719
[4] Connor J W 1995 *Plasma Phys. Controlled Fusion* **37** A119
[5] ITER Physics Basis 1999 *Nucl. Fusion* **39**
[6] Hidalgo C 1995 *Plasma Phys. Controlled Fusion* **37** 53
[7] Bak P, Tang C and Wiesenfeld K 1987 *Phys. Rev. Lett.* **59** 381
[8] Kadanoff L P *et al* 1989 *Phys. Rev.* A **39** 6524
[9] Hwa T and Kardar M 1992 *Phys. Rev.* A **45** 7002
[10] Politzer P A 2000 *Phys. Rev. Lett.* **84** 1192
[11] Pedrosa M A *et al* 1999 *Phys. Rev. Lett.* **82** 3621
[12] Carreras B A *et al* 1998 *Phys. Rev. Lett.* **80** 4438
[13] Carreras B A *et al* 1998 *Phys. Plasmas* **5** 1206
[14] Carreras B A *et al* 1998 *Phys. Plasmas* **5** 3632
[15] Carreras B A *et al* 1999 *Phys. Plasmas* **6** 485
[16] Carreras B A *et al* 1999 *Phys. Plasmas* **6** 4615
[17] Wang W H *et al* 2001 *Chin. Phys.* **10** 139
[18] Krommes J A and Ottaviani M 1999 *Phys. Plasmas* **6** 3731
[19] Krommes J A 2000 *Phys. Plasmas* **7** 1752
[20] Diamond P H and Hahm T S 1995 *Phys. Plasmas* **2** 3640
[21] Carreras B A, Newman D, Lynch V E and Diamond P H 1996 *Phys. Plasmas* **3** 2903
[22] Sarazin Y, Garbet X, Ghendrih P and Benkadda S 2000 *Phys. Plasmas* **7** 1085
[23] Garbet X and Waltz R E 1998 *Phys. Plasmas* **5** 2836
[24] Newman D, Carreras B A, Diamond P H and Hahm T S 1996 *Phys. Plasmas* **3** 1858
[25] Medvedev M V, Diamond P H and Carreras B A 1996 *Phys. Plasmas* **3** 3745
[26] carbone V *et al* 2000 *Phys. Plasmas* **7** 445
[27] Antoni V *et al* 2001 *Phys. Rev. Lett.* **87** 045001
[28] Daubechies I 1988 *Commun. Pure Appl. Math.* **41** 901
[29] Carreras B A *et al* 1999 *Phys. Rev. Lett.* **83** 3653
[30] Hurst H E 1951 *Trans. Am. Soc. Civ. Eng.* **116** 770
[31] Ritz Ch P *et al* 1988 *Rev. Sci. Instrum.* **59** 1739
[32] Wootton A J 1990 *J. Nucl. Mater.* **176**&**177** 77
[33] Lopes Cardozo N J 1995 *Plasma Phys. Controlled Fusion* **37** 799
[34] Soler M and Callen J D 1979 *Nucl. Fusion* **19** 703
[35] Ryter F *et al* 2001 *Phys. Rev. Lett.* **86** 2325
[36] Ryter F *et al* 2001 *Phys. Rev. Lett.* **86** 5498
[37] Hoang G T *et al* 2001 *Phys. Rev. Lett.* **87** 125001
[38] Nielsen A H, Pecsell H L and Juul Rasmussen J 1996 *Phys. Plasmas* **3** 1530
[39] Antar G *et al* 2001 *Phys. Rev. Lett.* **87** 065001
[40] Antar G, Devynck P, Garbet X and Luckhardt S 2001 *Phys. Plasmas* **8** 1612
[41] Sanchez E *et al* 2000 *Phys. Plasmas* **7** 1408
[42] Z S J and Medley S S 1989 *Phys. Fluids* B **1** 2058
[43] Maqueda R *et al* 2001 *Rev. Sci. Instrum.* **72** 931